Investigation of the Impact of High Concentration LiTFSI Electrolytes on Silicon Anodes with Reactive Force Field Simulations

– Supplementary Information –

Heather Cavers [1,3,‡], Julien Steffen [2,4,‡], Neeha Gogoi [1,5], Rainer Adelung [1], Bernd Hartke [2] and Sandra Hansen [1]

[1] University of Kiel, Institute for Material Science, Kaiserstr. 2, 24143, Kiel, Germany

[2] University of Kiel, Institute for Physical Chemistry, Max-Eyth-Str. 2, 24118 Kiel, Germany

[3] Technical University of Braunschweig, Institute for Particle Technology, Volkmaroder Str. 5, 38104, Braunschweig, Germany

[4] Friedrich Alexander University Erlangen-Nürnberg, Department of Chemistry and Pharmacy, Egerlandstraße 3, 91058 Erlangen, Germany

[5] Uppsala University, Department of Chemistry, 752 36 Uppsala, Sweden

[‡] These authors had equal contribution.

Contents

1 Force Field Optimization **2**

1.1 Training Set 2

1.2 Results 2

2 Molecular Dynamics Setup **9**

2.1 Electrolyte Buildup 9

2.2 Battery Establishment 11

3 Molecular Dynamics Results **12**

3.1 Element Distributions 12

3.2 Variation of Temperature and Pressure 15

3.3 Bond Distributions 19

3.4 Molecules 23

4 Experimental Results **30**

1 Force Field Optimization

1.1 Training Set

The structures and energy scans which were part of the training set to optimize the new ReaxFF force field are listed in this section. For the targeted optimization of these parameters it is important to define a reliable training set that includes the newly introduced coordinates in a number of chemical situations which have (mostly judging from intuition) a sufficient probability of occurring during the simulations near the surface. A list of small molecules that were thought to appear (at least as (here hydrogen-saturated) parts of larger structures) during the reactive dynamics is shown in fig. S1. The optimized ReaxFF force field should be able to reproduce the structures of these molecules as good as possible. Note that during ReaxFF parameter fitting, local geometry optimizations are performed for each new trial parameter set. This is computationally costly but ensures agreement of minimum-energy structures better than, e.g., minimizing interatomic forces for given structures.
In the second part, coordinate scans of the newly introduced bonds and angles listed in the main publication were done as reference for the optimization of the quantitative description of the energy profiles. For this, certain coordinates of the molecules in fig. S1 were scanned with the chosen DFT functional and basis set (see main publication). The scanned coordinates are shown in fig. S2. The atoms constituting the coordinates are highlighted with red circles. As can be seen, four scans of the Si-S bond length were included, complying with the fact that a correct description of all bond dissociation potentials is much more important for the description of reactive dynamics than those of angle potentials.

1.2 Results

In this section, the quality of the optimized ReaxFF force field is investigated in more detail. This is shown for the geometry part in fig. S3. Most bond lengths are reproduced well (less than 0.1 Å deviation), building four clusters at 0.95, 1.1, 1.5 and 1.7 Å, a small fraction shows larger deviations, up to 0.9 Å. This indicates, however, that all structures are stable and no dissociations occur. For bond angles, the average deviations are between 10 and 15 degrees, but no outlier are present here, in contrast to the bond lengths. Therefore, also angles are reproduced reasonably. The dihedral angles are reproduced with good quality, showing somewhat smaller deviations than bond angles, around 10 degrees. In summary, the reproduction of the geometries is reasonable, albeit not of outstanding quality.
The quality of the optimized ReaxFF with respect to the energetics of the system (bond- and angle scans) is shown in figs. S4-S6. The S-Si bond length profiles (S1-S4) show qualitative

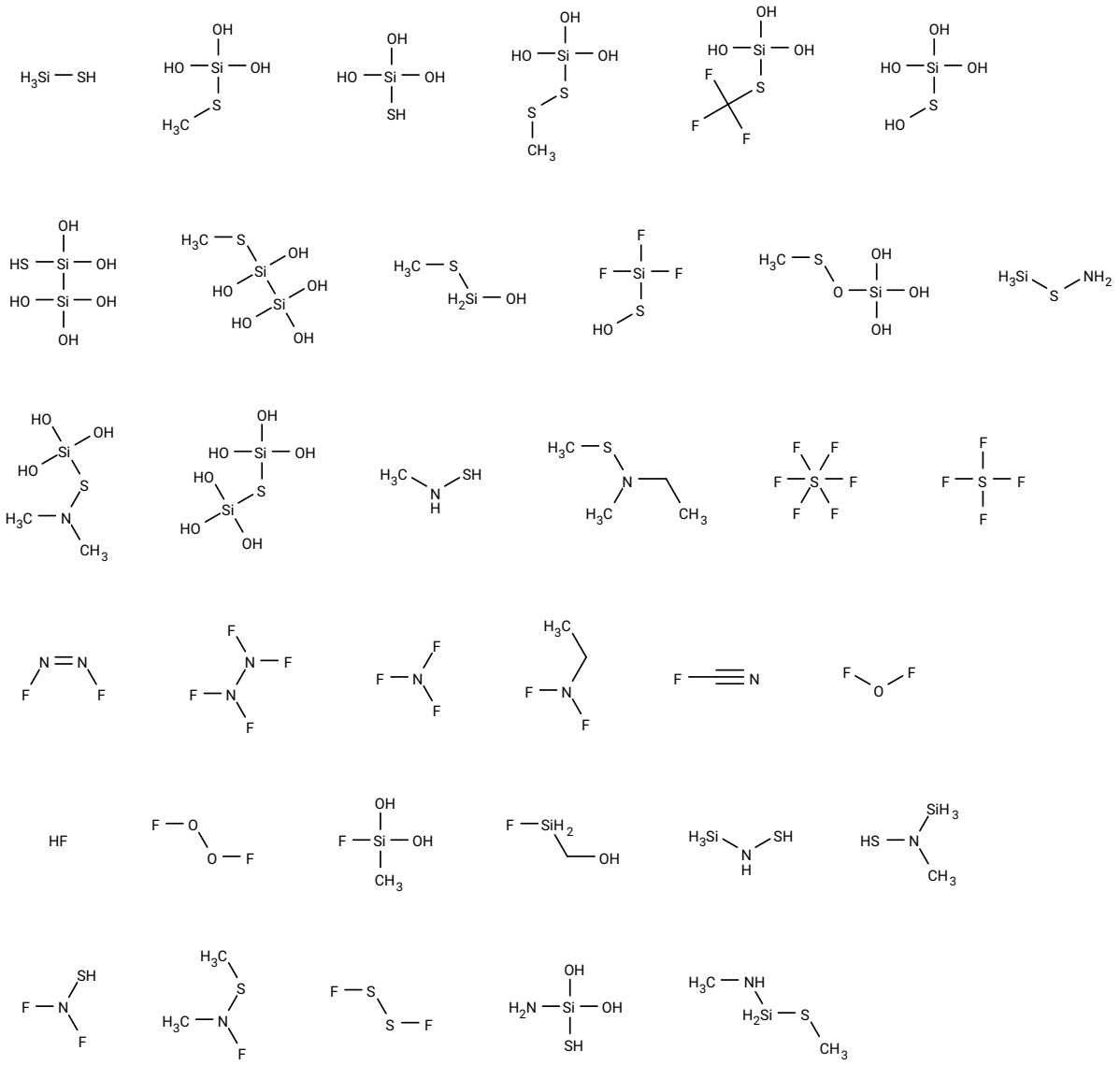

Figure S1: Schematic overview of all molecules contained in the coordinate part of the training set.

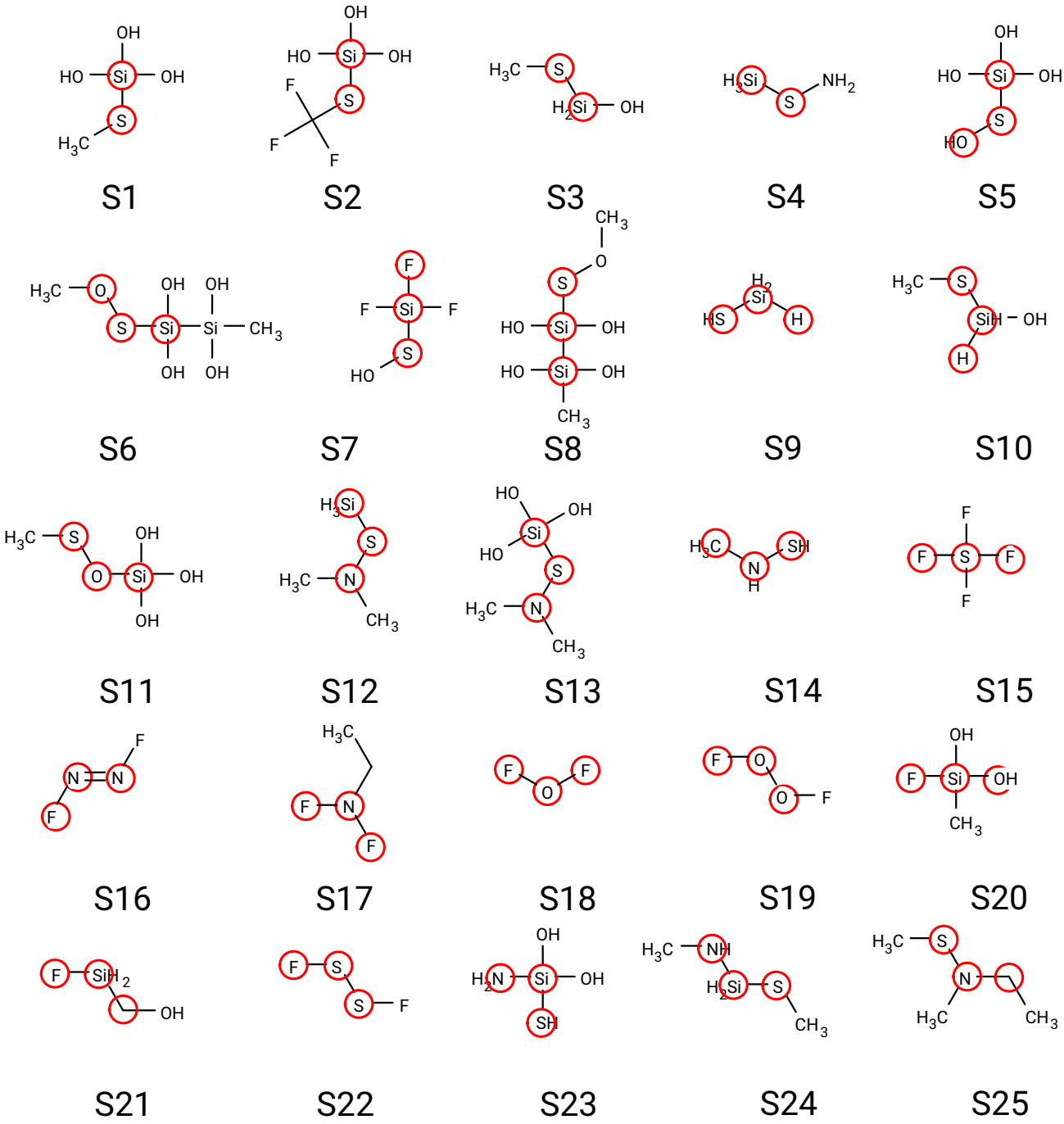

Figure S2: Schematic overview of all bond/angle scan coordinates contained in the energetic part of the training set.

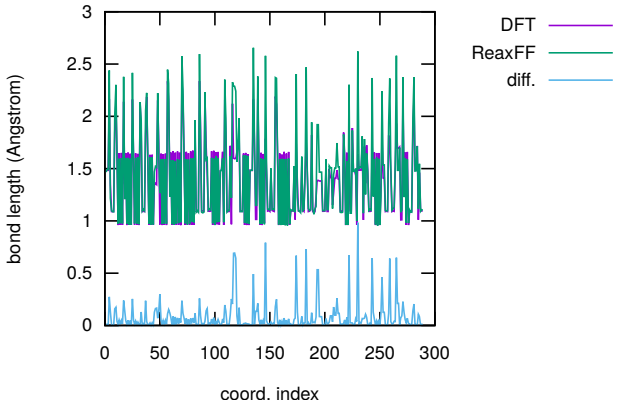

(a) Bond lengths

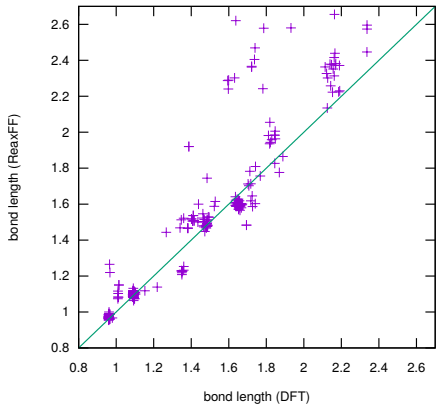

(b) Bond lengths

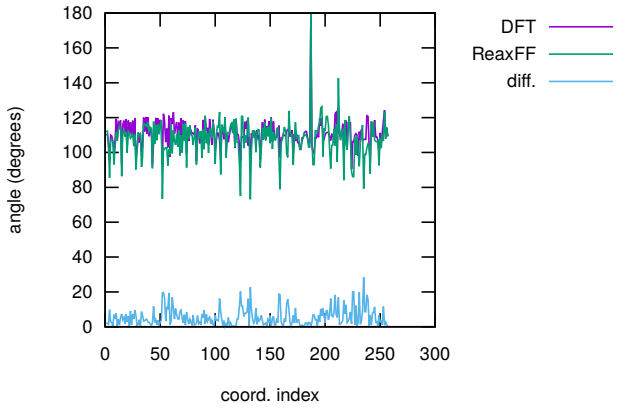

(c) Angles

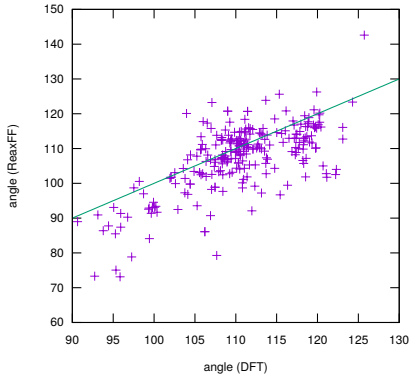

(d) Angles

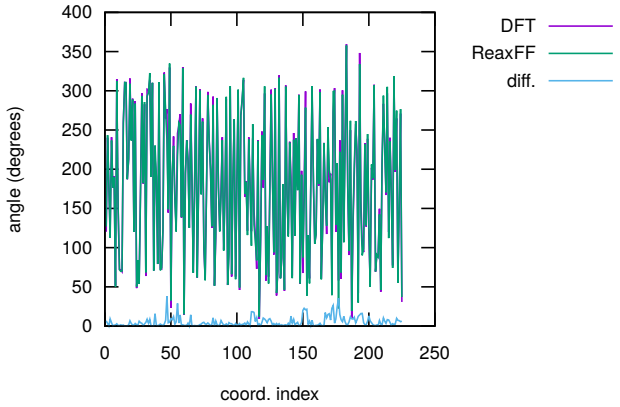

(e) Dihedrals

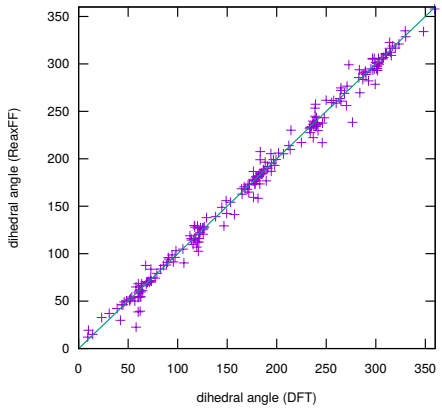

(f) Dihedrals

Figure S3: Results of the OGOLEM ReaxFF parameter optimization for the geometry part of the training set. Shown are the deviations between ReaxFF and DFT reference for all included coordinates, where the ReaxFF values originate from geometry optimized structures (fig. S1) with the optimized force field.

agreement, although their shapes are quite different. The ReaxFF curves have a much narrower minimum and reach their dissociation energy at approx. 3.5 Å, whereas the DFT curves converge much slower. The qualitative characteristics, however, are reproduced satisfactorily. The equilibrium ReaxFF equilibrium lengths are somewhat larger than the DFT references, but the absolute deviation is only around 0.1 Å. The dissociation energies deviate between 50 and 60 kJ mol^{-1}, Sc4 shows a deviation around 100 kJ mol^{-1}, but with the kink near the dissociation somewhat complicating the system.

The angle scans show quite a variety of behaviors. ReaxFF shows very satisfying quality for some of them (Sc8, Sc18, Sc21, Sc23), whereas other profiles show large deviations in the energetics (Sc7, Sc11, Sc14, Sc25). Most of them, however, reproduce a correct equilibrium angle and do not diverge.

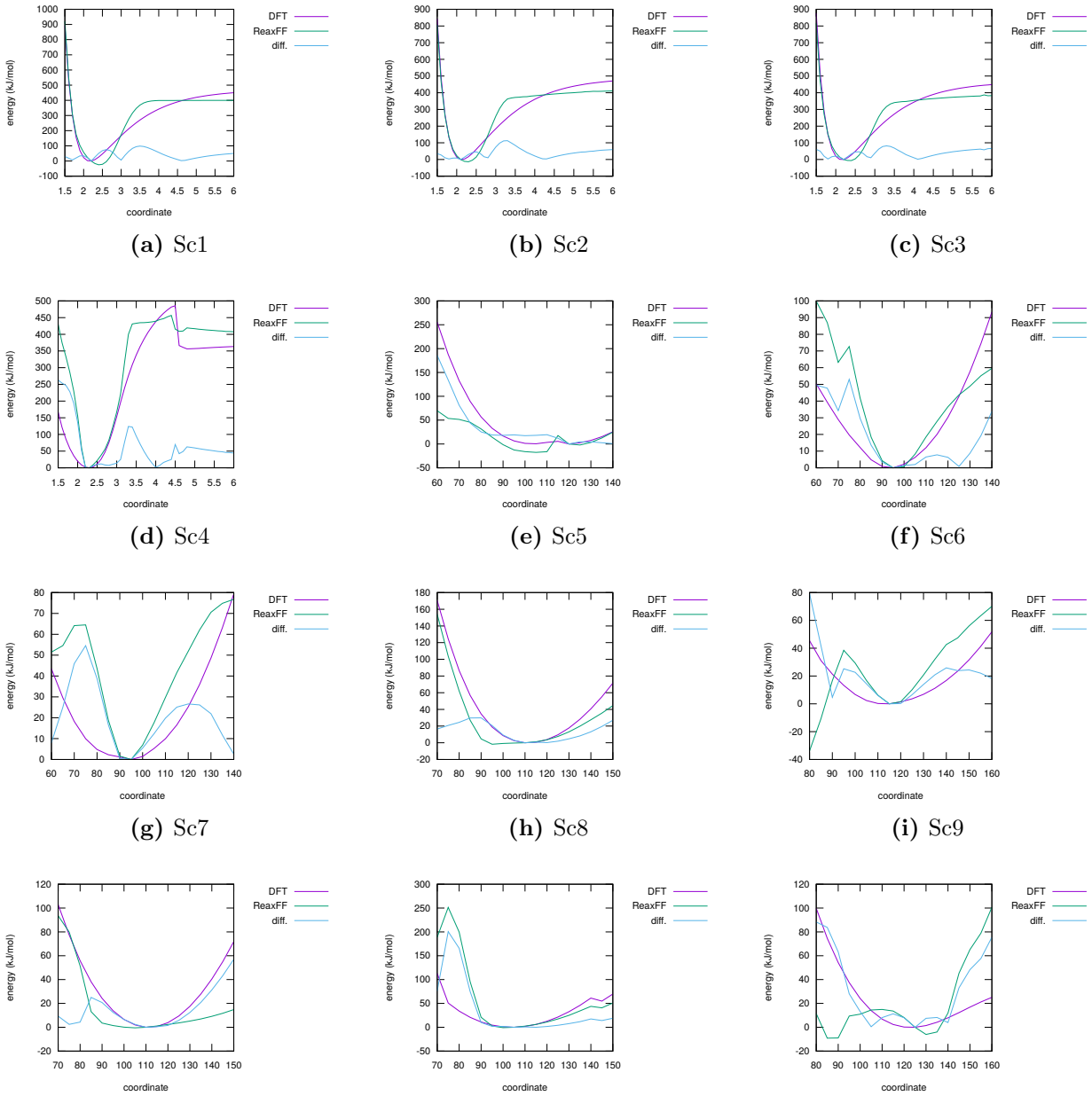

(a) Sc1 **(b)** Sc2 **(c)** Sc3

(d) Sc4 **(e)** Sc5 **(f)** Sc6

(g) Sc7 **(h)** Sc8 **(i)** Sc9

(j) Sc10 **(k)** Sc11 **(l)** Sc12

Figure S4: Results of the OGOLEM parameter optimization for the first twelve energy scans in the training set. The first four scans are bond lengths. See fig. S2 for the actual structures. Three curves are shown for each scan: (DFT) the DFT reference, (ReaxFF) the optimized ReaxFF and (diff.) the difference between them.

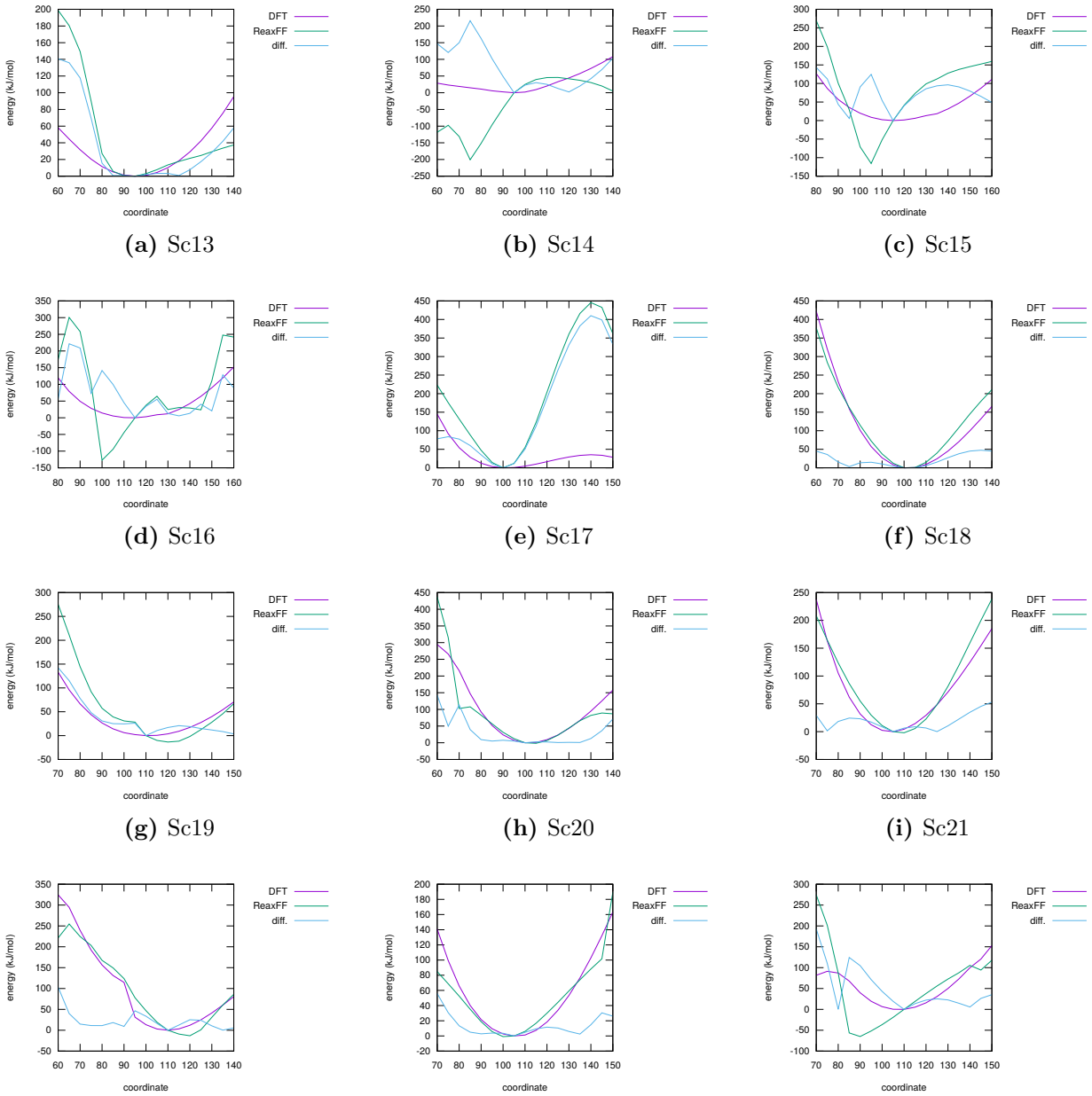

(a) Sc13 **(b)** Sc14 **(c)** Sc15

(d) Sc16 **(e)** Sc17 **(f)** Sc18

(g) Sc19 **(h)** Sc20 **(i)** Sc21

(j) Sc22 **(k)** Sc23 **(l)** Sc24

Figure S5: Results of the OGOLEM parameter optimization for the second twelve energy scans in the training set. See fig. S2 for the actual structures. Three curves are shown for each scan: (DFT) the DFT reference, (ReaxFF) the optimized ReaxFF and (diff.) the difference between them.

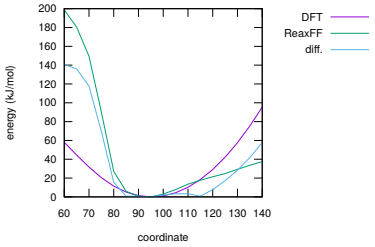

(a) Sc25

Figure S6: Results of the OGOLEM parameter optimization for the 25th energy scan in the training set. See fig. S2 for the actual structures. Three curves are shown for each scan: (DFT) the DFT reference, (ReaxFF) the optimized ReaxFF and (diff.) the difference between them.

2 Molecular Dynamics Setup

2.1 Electrolyte Buildup

Here, the setup of the model system is explained step by step. All calculations presented here and in the following were done with the LAMMPS molecular simulation package. First, single boxes of DOL and DME were prepared with the script `box_lammps.pl`, which we developed and is able to generate the LAMMPS input file for a crystalline box of molecules, if LAMMPS input for the single molecules are given.

The single boxes with pure DOL and DME were set up with 512 molecules each and were equilibrated with the NpT ensemble at 1 bar pressure and 298 K. The obtained averaged volumes (after the box size converged) were 61685 $\mathring{A}^3$ (DOL) and 86077 $\mathring{A}^3$ (DME), which results in a translation of the 1:2 (v/v) ratio of DOL and DME to a molecular number ratio of 1:1.39544 (mol/mol).

With this as prerequisite, a formula for conversion of LiTFSI molecular ratio to LiTFSI concentration can be fitted. A cubic simulation box with 1000 molecules in total and different LiTFSI fractions was set up (see table S1). After performing 1 ns of NpT dynamics each, the LiTFSI concentrations were obtained from the averaged box volumes after equilibration. These are also noted in the table.

A satisfying conversion function from desired concentration to LiTFSI fraction was found after fitting to the data:

$$x(c) = -\frac{1}{2a_2} + \sqrt{\frac{1}{2a_2} - \frac{1}{a_2^2}\left[a_3 - \exp\left(\frac{c - a_4}{a_1}\right)\right]}, \tag{S1}$$

with the optimized parameters $a = 0.544172$, $b = 68.1394$, $c = 0.816673$, $d = 0.181978$.

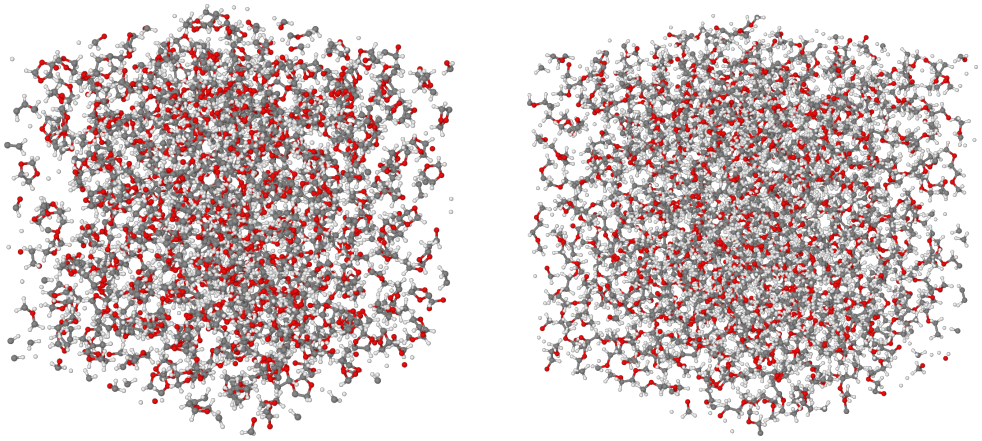

(a) DOL **(b)** DME

Figure S7: The equilibrated boxes with DME and DOL molecules.

Table S1: Compositions of different solvent boxes with 1000 molecules in total as used for the concentration function.

run	ratio of molecules			LiTFSI concentration (mol L^{-1})
	DOL	DME	LiTFSI	
1	1.0	1.39544	0.01	0.06467
2	1.0	1.39544	0.05	0.23581
3	1.0	1.39544	0.2	0.84747
4	1.0	1.39544	0.5	1.82662
5	1.0	1.39544	1.0	2.47808
6	1.0	1.39544	1.5	3.05467

With this information, the final setup for the electrolyte part could be done. Since one is interested in properties along the SEI, it was decided to build a lengthy box with elongated z-axis. The regular mesh setup consisted of 7x7x20 molecules (x, y, z directions). With this, the 0.7 M LiTFSI system consists of 384 DOL, 536 DME and 60 LiTFSI molecules, whereas the 4 M TFSI system consists of 228 DOL, 324 DME and 428 LiTFSI molecules.
Both boxes were equilibrated with NpT dynamics (1 bar), at 298 and 700 K (for the high-temperature experiments, see below). Besides obtaining a realistic representation of the electrolyte solutions, the whole setup served another purpose: verifying if the ReaxFF is stable. Since bonding patterns are not predefined (in contrast to OPLS), a bad parametrization can lead to unstable molecules and explosions at temperatures where no such behavior should be expected. According to our prior ReaxFF optimization experience, such instabilities occur fairly quickly and are hard to miss. Fortunately, no such events were recorded during the whole setup process, indicating a solid and reliable behavior of the optimized ReaxFF in describing pure

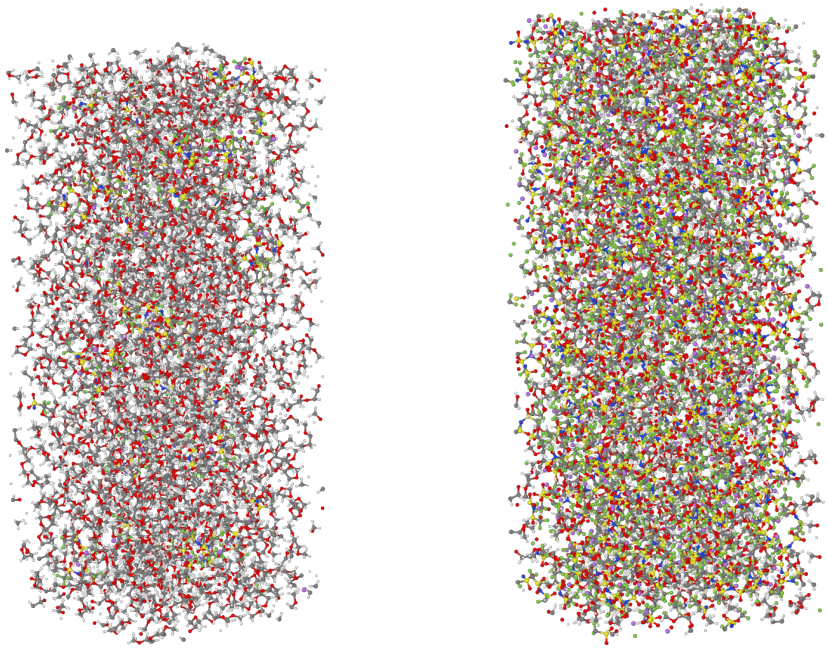

(a) 0.7 M **(b)** 4 M

Figure S8: The equilibrated boxes with DME and DOL molecules.

electrolyte solutions.

2.2 Battery Establishment

All what remained is plugging together the electrolyte solutions with the silicon oxide anodes. This was done with the script `silicon_surface.pl`, written during our studies. A longer explanation to this is provided in the main text.
The anode consists of 6272 atoms in both systems, leading to a total system size of 19113 atoms for the 0.7 M LiTFSI battery and 19826 atoms for the 4 M LiTFSI battery.

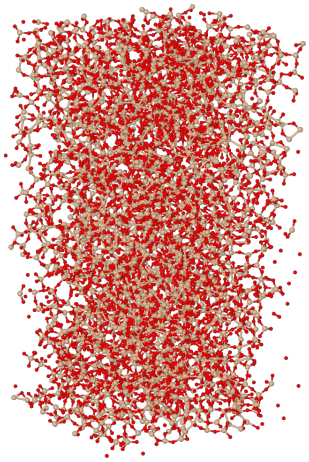

Figure S9: Screenshot of the equilibrated amorphous SiO_2 anode.

3 Molecular Dynamics Results

In this chapter, the resulting MD trajectories of the different model batteries will be analyzed with much detail, whereas the general structure from the main publication is retained.
The plots were generated with the program `reax_eval`, written by us, which is specially designed for battery interface systems but is independent of the exact composition of electrolyte/electrode, such that SEI formation processes of other Li-ion battery systems could be evaluated with it as well. Before showing the different results, their processing is explained shortly as well.

3.1 Element Distributions

The simplest analysis is to look, independent of chemical bonding, how the nine different elements present in this system are distributed in space. Since we are interested mainly in the direction perpendicular to the SEI interface, i.e., the z-axis, the `reax_eval` program packed all atoms of the respective elements in the system into 200 bins along the z-axis, separately for each written time step (one per ps, i.e., 1400 frames in total).
The results of this procedure are shown in fig. S10 for the 0.7 M TFSI system. As expected, two parts of the whole system can be easily identified: The SiO_2 anode at $z = -20$ to $z = 50$, where both silicon and oxygen concentrations are high, and the electrolyte at $z = 50$ to $z = 140$, where all elements apart from silicon are present (oxygen with lower concentration than in the SiO_2 bulk).
The most interesting part for us is of course the interface between electrolyte and anode (at $z \approx 50$). A mixing region between both faces is established successively, up to 500 ps the abundancies of all elements except silicon trickle some Å to lower regions, building up an

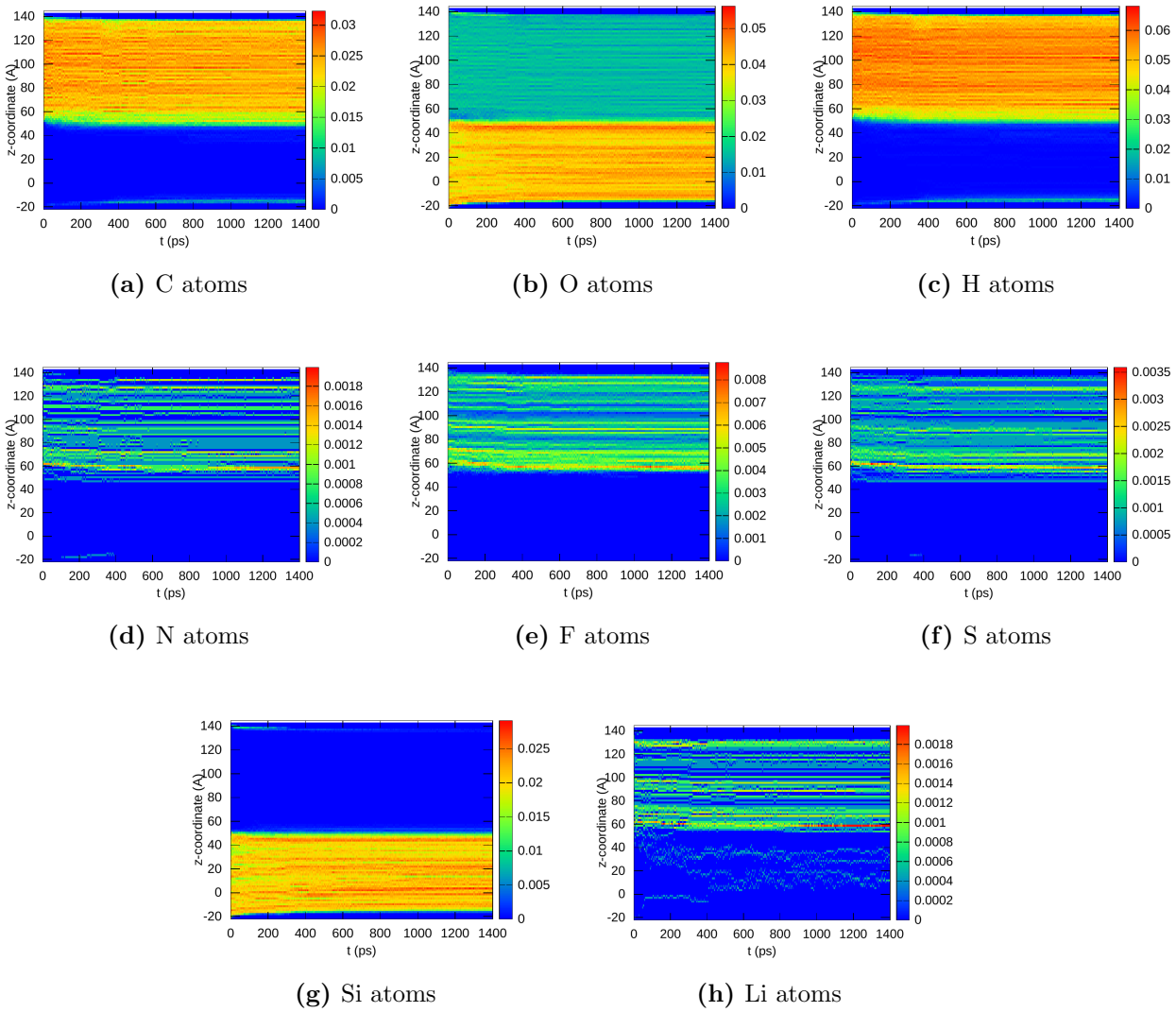

(a) C atoms **(b)** O atoms **(c)** H atoms

(d) N atoms **(e)** F atoms **(f)** S atoms

(g) Si atoms **(h)** Li atoms

Figure S10: z-coordinate and time-dependent element distribution in the 0.7 M Li-ion battery system.

interface with medium concentrations between $z = 45$ and $z = 55$. This intermediate region can be identified as SEI, as other results presented below will affirm.

Note that the system is periodic in z-direction, such that atoms might disappear in the lower border and reappear in the upper border.

The same analysis was done for the 4 M TFSI system (fig. S11). It becomes obvious at first sight that the SEI region(s) is (are) now much broader. It covers approximately 20 Å on both sides of the anode ($z = 40$ to z_60 and $z = -30$ to $z = -10$). Due to the higher number of TFSI ions, the density of F atoms is now almost smooth, instead of consisting of single filaments as in the 0.7 M case above. N and S atoms, that only appear once/twice in each TFSI molecule, still

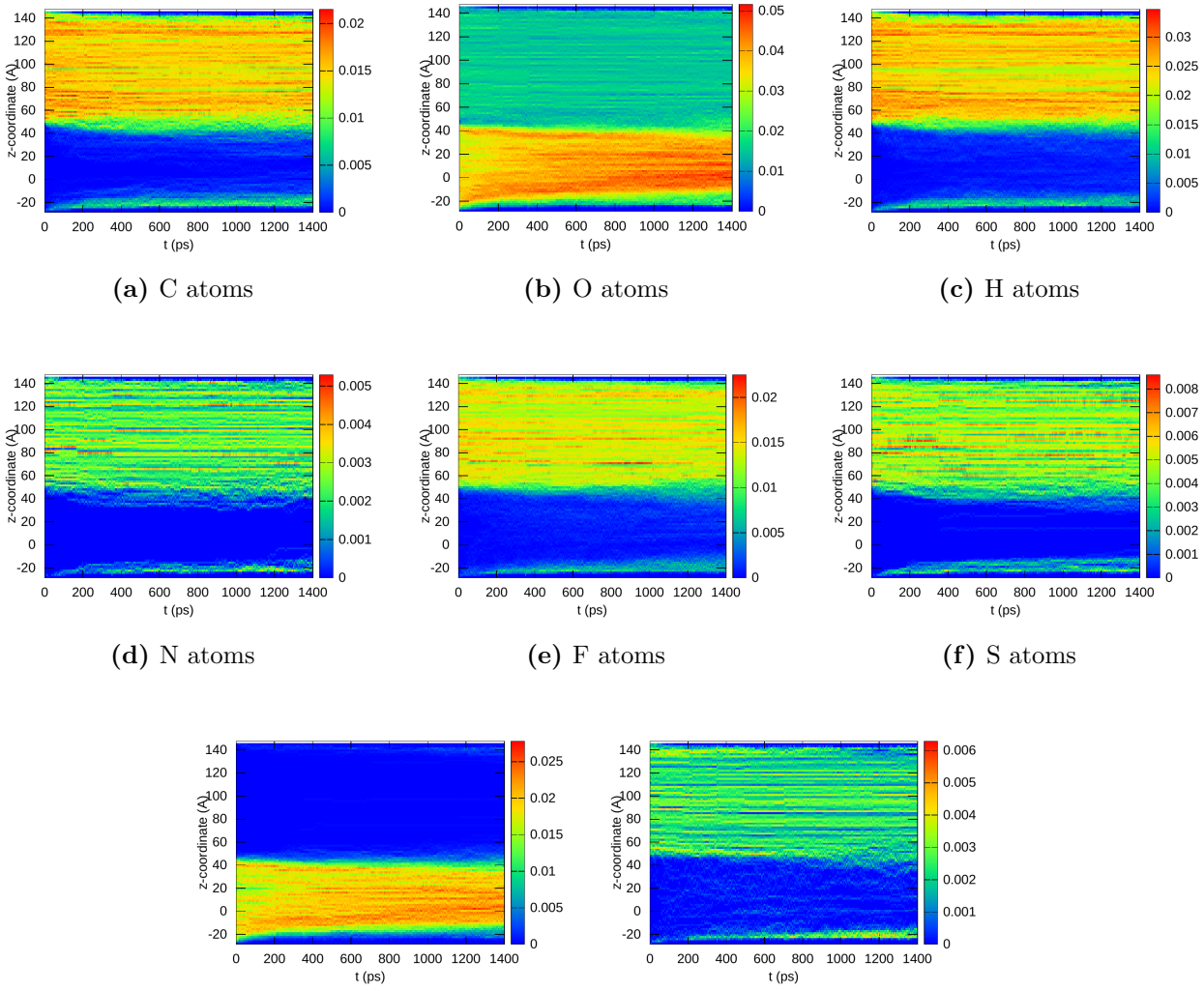

(a) C atoms **(b)** O atoms **(c)** H atoms

(d) N atoms **(e)** F atoms **(f)** S atoms

(g) Si atoms **(h)** Li atoms

Figure S11: z-coordinate and time-dependent element distribution in the 4 M Li-ion battery system.

show some fine-structure in their densities.

Besides the intermixed SEI, Li, H, F and C atoms can be found in the whole anode material at the end of the dynamics, indicating that there is indeed a two stage SEI, where the second stage deeply penetrates the anode material itself. Silicon atoms, on the other hand, do not penetrate into the electrolyte phase, indicating that the anode plays the role of a sponge that sucks significant portions of the electrolyte (or rather its reaction/decomposition products) into it.

3.2 Variation of Temperature and Pressure

A popular method to extend the effective time scale of reactive molecular dynamics is to raise the simulation temperature. In order to study whether this approach might be useful for the current simulations, all calculations were redone with a temperature of 700 K. This is shown in fig. S12 for the distributions of C, S and Li and both LiTFSI concentrations. The results for 0.7 M are quite chilling: The electrode and electrolyte phases seem to decompose completely at 700 K, it seems that the whole structure becomes unstable. The 4 M systems behaves more stable, by keeping both phases essentially intact, the growth of the SEI is significantly accelerated, a sulfur-rich intermediate phase at $z \approx 30$ is formed.
Another approach was to raise the pressure of the system from 1 bar to 1000 bar and see whether this leads to a significant increase of reaction rates (by simultaneously maintaining the overall mechanisms and stochiometry). This is shown for the 0.7 M TFSI system in fig. S13 for C, S and Li. All combinations of 298, 700 K and 1, 1000 bar were tried. The main finding is that the significant pressure difference hardly has any impact on the results, which is quite surprising but might originate, e.g., in the ionic nature of the system. The width of the SEI seems slightly narrower for 1000 bar at 298 K, but no overall different behavior can be detected.
The results for the 4 M system in fig. S14 support these findings. Pressure changes interestingly make almost no difference for the 298 K system, the most significant observation is that the concentration of Li ions within the anode seems to be somewhat higher for 1000 K. The 700 K distributions again show an unexpected sulfur concentration band in the SEI region.
In total, it can be stated that both temperature and pressure change had no positive impact on the dynamics. Whereas the former seems to ruin the whole dynamics, the latter has no visible impact as all. The objective of accelerating the dynamics by keeping its chemical progress unchanged was clearly missed. Since the simulated reaction time was clearly sufficient for the 0.7 M system and a meaningful part of the reactions seem to reach a converged state at 4 M, it was decided to only evaluate the simulations at standard conditions for the remainder of our studies.

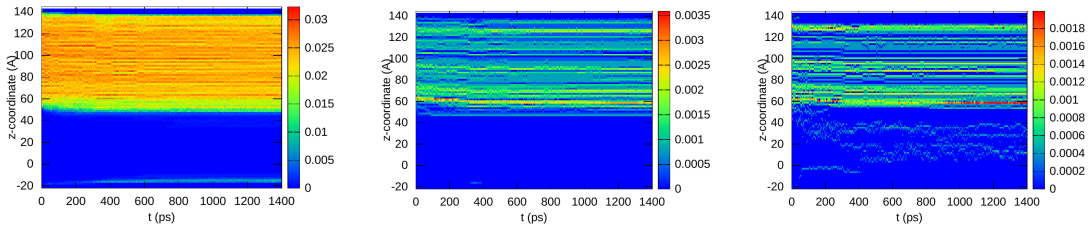

(a) C, 0.7M, 300K **(b)** S, 0.7M, 300K **(c)** Li, 0.7M, 300K

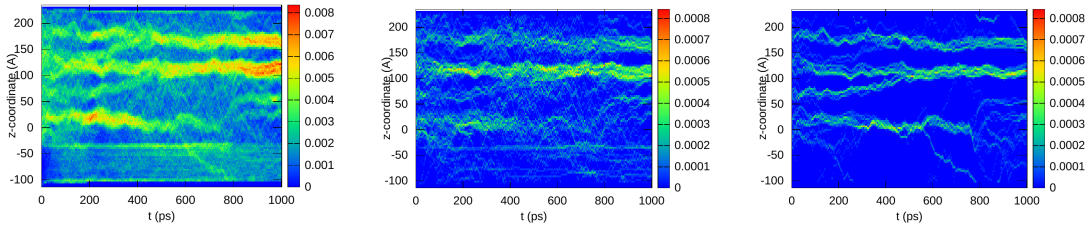

(d) C, 0.7M, 700K **(e)** S, 0.7M, 700K **(f)** Li, 0.7M, 700K

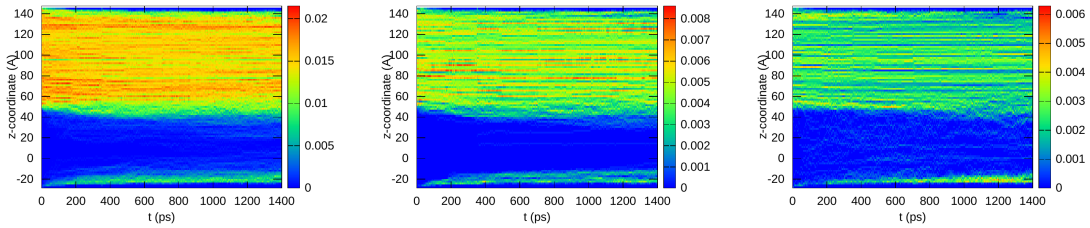

(g) C, 4M, 300K **(h)** S, 4M, 300K **(i)** Li, 4M, 300K

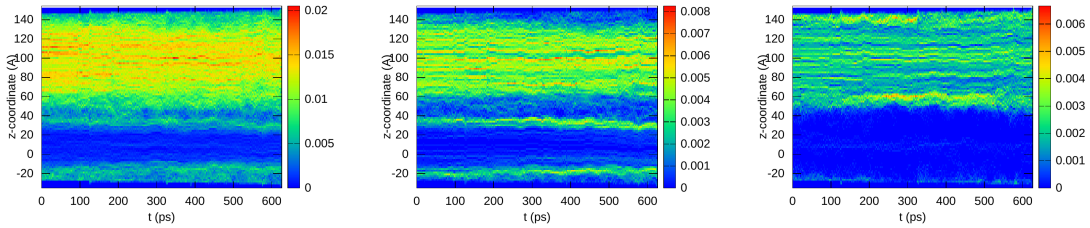

(j) C, 4M, 700K **(k)** S, 4M, 700K atoms **(l)** Li, 4M, 700K

Figure S12: Element distributions for C, S and Li for two different simulation temperatures (300 K and 700 K).

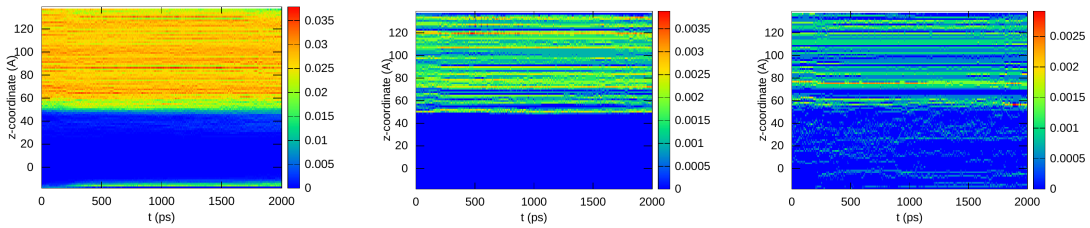

(a) C, 300K, 1bar **(b)** S, 300K, 1bar **(c)** Li, 300K, 1bar

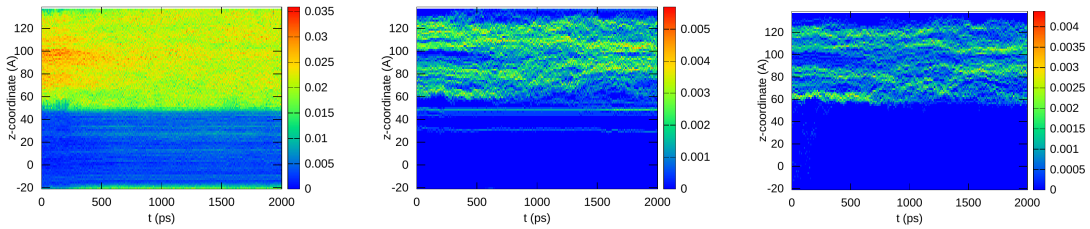

(d) C, 700K, 1bar **(e)** S, 700K, 1bar **(f)** Li, 700K, 1bar

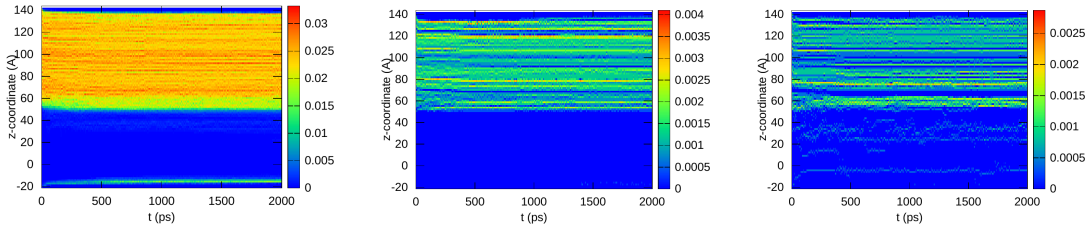

(g) C, 300K, 1000bar **(h)** S, 300K, 1000bar **(i)** Li, 300K, 1000bar

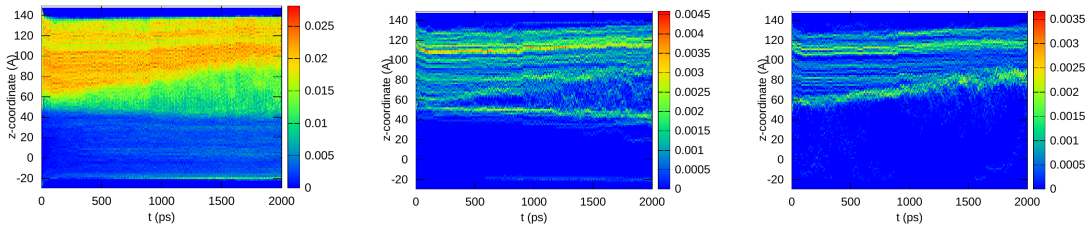

(j) C, 700K, 1000bar **(k)** S, 700K, 1000bar **(l)** Li, 700K, 1000bar

Figure S13: Element distributions for C, S and Li (0.7 M LiTFSI) for two different simulation temperatures (300 K and 700 K) and pressures (1 bar and 1000 bar).

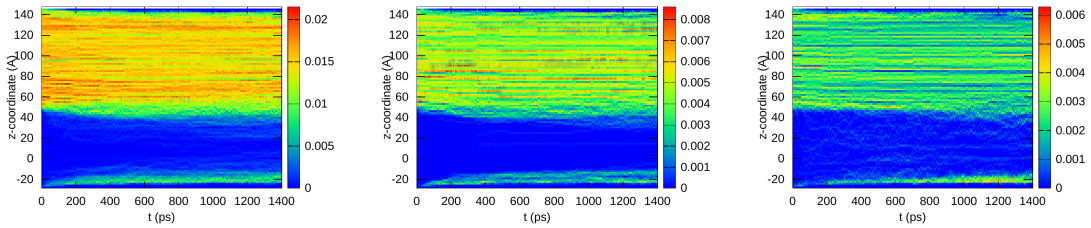

(a) C, 300K, 1bar **(b)** S, 300K, 1bar **(c)** Li, 300K, 1bar

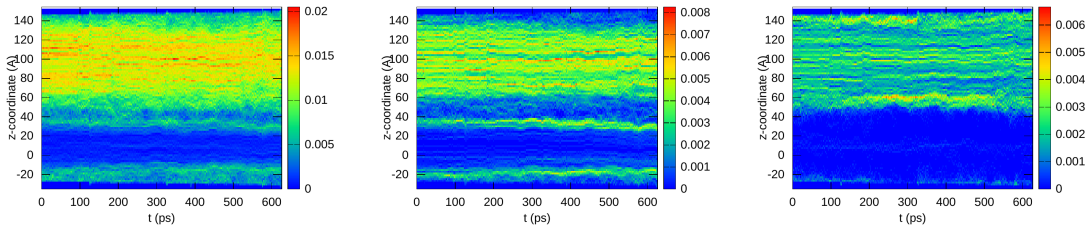

(d) C, 700K, 1bar **(e)** S, 700K, 1bar **(f)** Li, 700K, 1bar

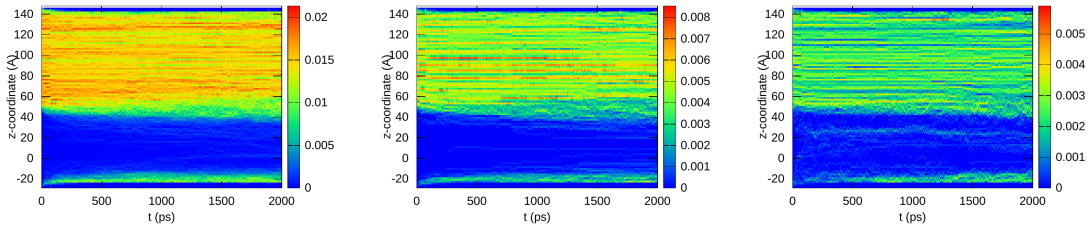

(g) C, 300K, 1000bar **(h)** S, 300K, 1000bar **(i)** Li, 300K, 1000bar

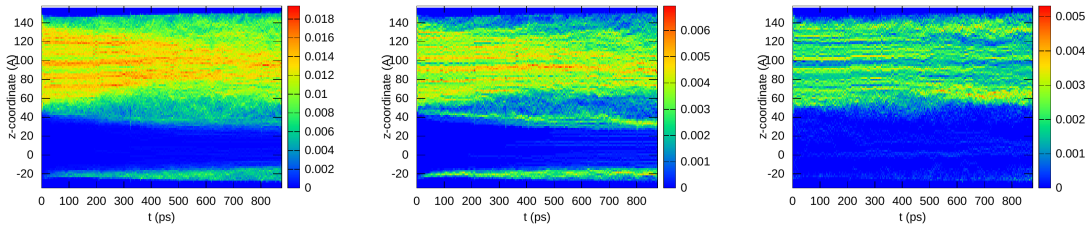

(j) C, 700K, 1000bar **(k)** S, 700K, 1000bar **(l)** Li, 700K, 1000bar

Figure S14: Element distributions for C, S and Li (4 M LiTFSI) for two different simulation temperatures (300 K and 700 K) and pressures (1 bar and 1000 bar).

3.3 Bond Distributions

It is also possible to assign chemical bonds to locations in space. This is simply done by determining the mid point of both involved atoms and defining this point as bond location. Now, space- and time resolved plots similar to those for the elements given above can be produced for the different bond species.

This is shown for the 0.7 M system in fig. S15 (due to the large number of possible bond combinations, only the most abundant ones are shown). There are two kinds of bonds: Those, which mainly exist within one phase (O-Si, C-H, C-O, Si-Si C-C, C-F and C-S) and those, which are newly formed in the SEI region at z=40-60 Å (H-O, C-Si, O-F, O-N, S-Si). The areas where the one-phase bonds occur grow during the first 100 ps, indicating a (initially mainly nonreactive) penetration of both phases. After 50-100 ps, the densities of the SEI bonds begin to grow until 200-300 ps, after which equilibrium seems to be reached. H-O bonds are much less concentrated in the narrow SEI region, instead they significantly penetrate into the anode material. Si-Si bonds vanish during the dynamics also within the anode bulk, which might indicate a further rearrangement of the crystal structure.

As already indicated by the total bond numbers, much more happens in the 4 M TFSI system. O-Si, C-H, C-O, C-C, C-F and C-S bonds remain almost entirely in their respective phases, widths of the O-Si and C-F regions shrink, indicating that these are consumed during the SEI buildup process, whereas C-H, C-O and C-S bonds seem to be reformed in the SEI regions. Newly formed bond species are H-O, C-Si (similar to the 0.7 M system), as well as O-F and S-Si, which were not relevant in the 0.7 M system. This indicates that the TFSI anions play a crucial role in the SEI builtup if their concentration is high enough.

Finally, the bond distributions in the first and last MD frame are plotted separately, as done for the elements as well (see main publication). The plots for 0 ps are quite uninteresting; as it could be expected, electrode and electrolyte phases are clearly separated. At 1.4 ns, much more can be seen: for the 0.7 M system, the bond distributions of both phases overlap between z=40 and z=60, in addition, new bonds like C-Si can be found there. In the zoomed plot (e), C-Si and H-O can be identified as main inter-phase-species, where the H-O distribution is somewhat more extended into the anode region (small z). O-F bonds, on the other hand, seem to be built mainly on the electrolyte side of the SEI (z=50 to z=60).

For the 4 M system, it is much harder to clearly separate the SEI region visually from the anode and electrolyte phases. The C-Si bonds can be found in the complete anode region, whereas the H-O bonds are present almost in the complete electrolyte region. It can be followed that the SEI is now much broader in total, its anode side consists mainly of C-Si bonds, the electrolyte side mainly of H-O and O-F bonds. Silicon atoms (and bonds between them) show almost no

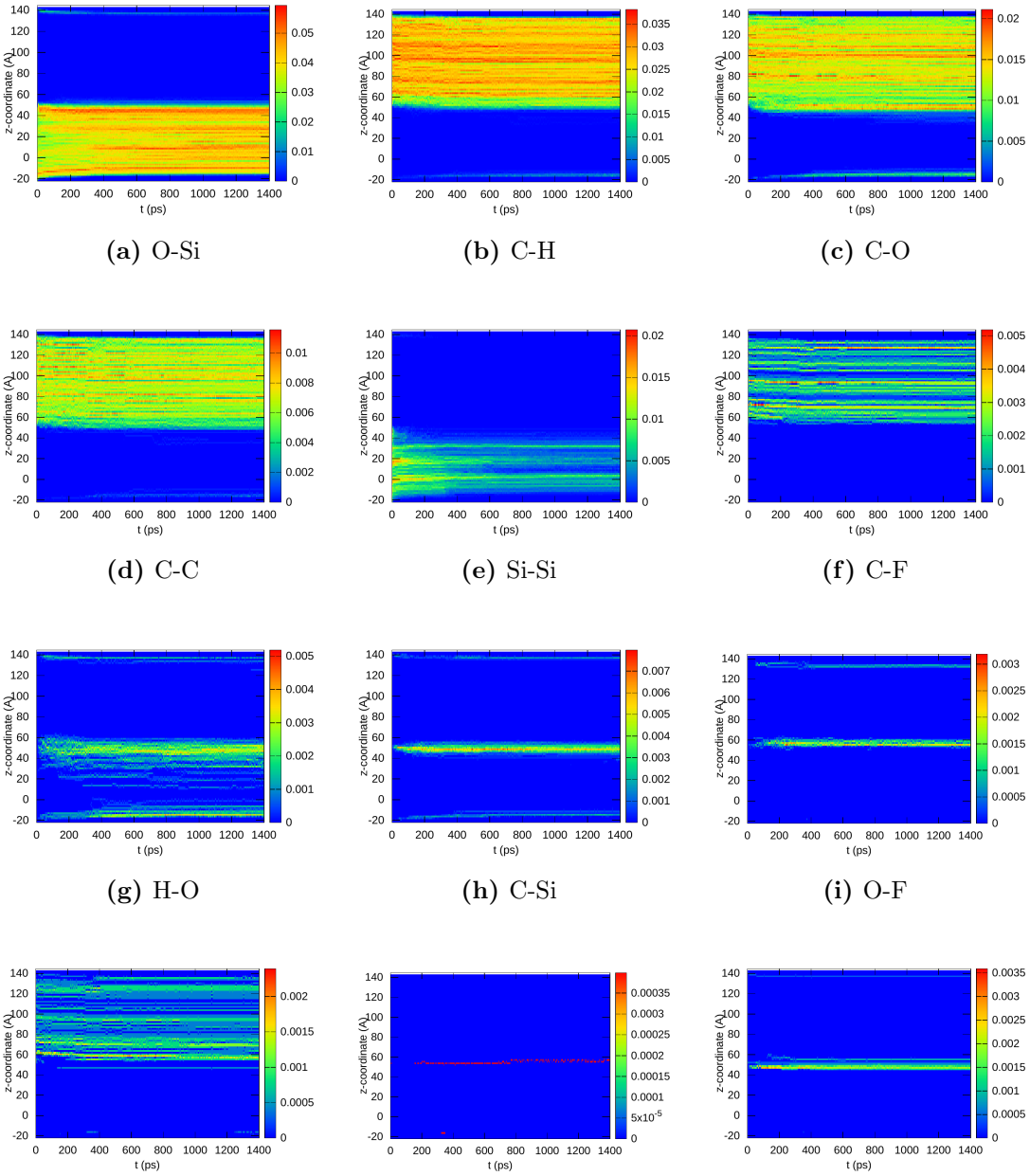

(a) O-Si **(b)** C-H **(c)** C-O

(d) C-C **(e)** Si-Si **(f)** C-F

(g) H-O **(h)** C-Si **(i)** O-F

(j) C-S **(k)** O-N **(l)** S-Si

Figure S15: Space- and time resolved densities of different bond species during the ReaxFF dynamics of the 0.7 M TFSI system. Shown are only bond species with largest total abundancy.

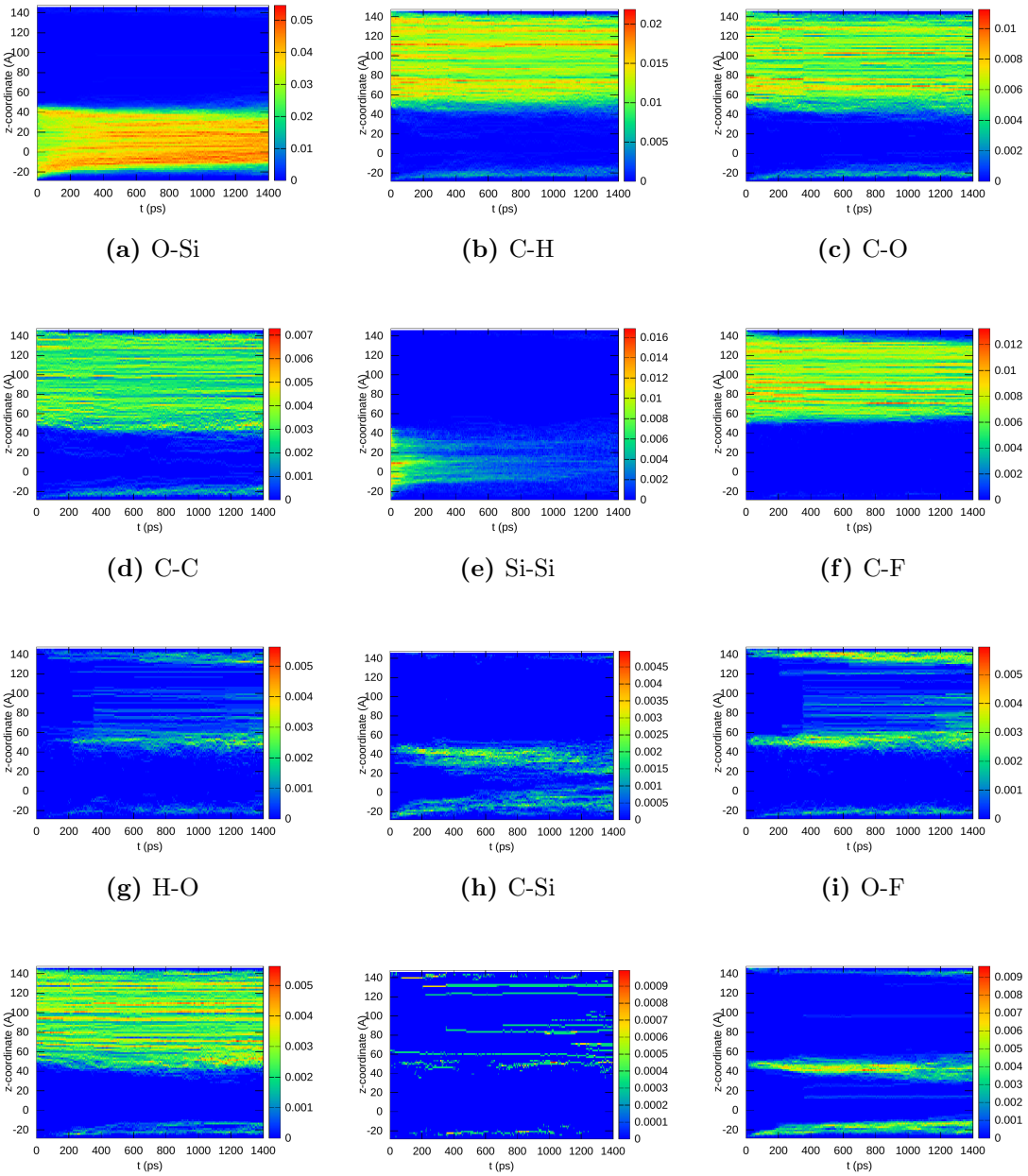

(a) O-Si **(b)** C-H **(c)** C-O

(d) C-C **(e)** Si-Si **(f)** C-F

(g) H-O **(h)** C-Si **(i)** O-F

(j) C-S **(k)** O-N **(l)** S-Si

Figure S16: Space- and time resolved densities of different bond species during the ReaxFF dynamics of the 4 M TFSI system. Shown are only bond species with largest total abundancy.

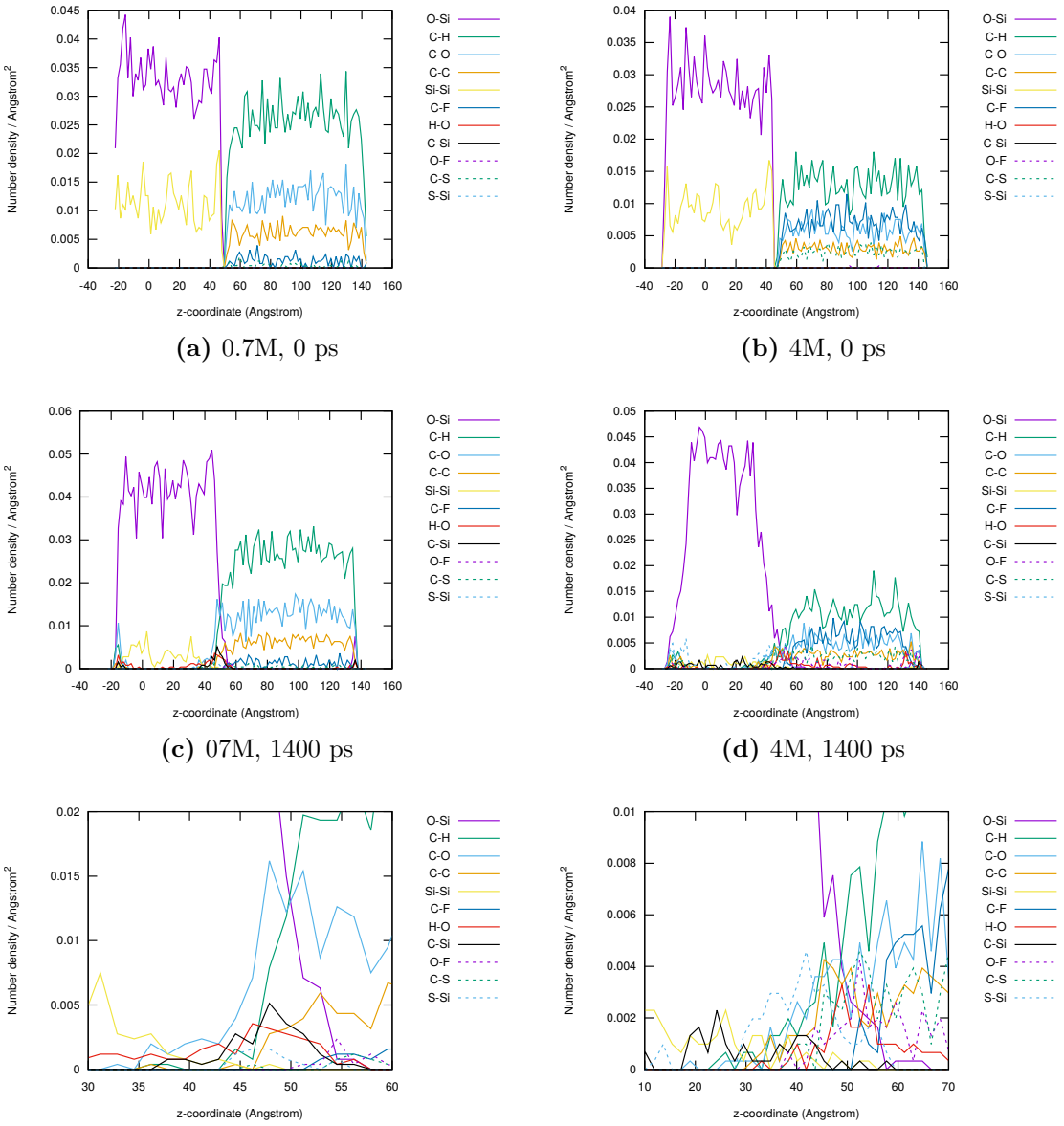

(a) 0.7M, 0 ps

(b) 4M, 0 ps

(c) 07M, 1400 ps

(d) 4M, 1400 ps

(e) 07M, 1400 ps, zoom

(f) 4M, 1400 ps, zoom

Figure S17: Bond concentrations along the z-axis at the first and last time step of the simulated systems with 0.7 and 4 M LiTFSI concentration.

tendency to leave the former anode region.

3.4 Molecules

The automatic identification of small molecules during the dynamics was implemented within our evaluation program `reax_eval`. Entry points are the lists of bonds written from LAMMPS which were already used for the bond analysis in the preceding chapter. A short overview of the central algorithm is given in scheme S1 in terms of pseudo-code.

Algorithm S1 Construction of Molecules

```
for i = 1, nframes do                                   ▷ Loop over MD frames
    for j = 1, nbonds do                                ▷ List of bonds in the actual frame
        Each bond is a possible starting point for molecules
        Skip, if one of the atoms is already used
        Store both atoms in new molecule and mark atoms as used.
        while True do                                   ▷ Loop over shells of actual molecule
            for k = 1, natoms_act do                    ▷ Loop over current atoms
                Loop through atoms currently present in molecule
                for l = 1, neighbor_num do              ▷ Loop over spatially close bonds
                    Loop though all bonds in the spatial vicinity
                    Possible cases: (both ends)
                    A: Atom 1 is part of molecule, 2 not: add atom 2
                    B: Atoms 1 and 2 belong to molecule: skip bond
                    C: Atom 1 already used before: delete molecule
                end for
            end for
            No new atoms added: finalize molecule
        end while
        Molecule ended: Correct for periodicity and write xyz file
        Generate SMILES S1 with openbabel
        Compare S1 with database 𝔻
            S1 ∈ 𝔻: Increment number of entry
            S1 ∉ 𝔻: Add new entry (number: 1)
    end for
end for
```

Each bond is a possible seed crystal for a new molecule: If none of the involved atoms is used in a previous molecule, both are added to the new molecule. Then an endless loop is started: For each atom in the molecule is is checked whether bonds exist in the surrounding that have the atom as one of its bond partners. This operation would scale heavily with system size if all bonds in the system would be checked in each iteration, therefore, a local list of nearest bonds is built before the algorithm is started. There, for each atom, a list of 50 nearest bonds (determined based on their center of mass, see section 6.3), is stored. If one of the surrounding bonds indeed contains an atom of the molecule, three cases can appear:

1. Atom 1 is part of the molecule and atom 2 not (or vice versa): add the missing atom
2. Both atoms belong to the molecule: skip the bond and do nothing
3. If the current atom already belongs to a previous molecule: delete the current molecule (in order to avoid double counting of molecules started from different ends)

After doing this for all atoms of the current molecule, a new loop is started, where the grown molecule containing the newly added bonds is looked at. When an entire loop ended and no new atoms were added, the molecule is considered as complete, as no dangling bonds remained. Alternatively, if the maximum allowed atom number in molecules is reached (7 in the current evaluations, with the focus on small gas species), the current molecule is finished and stored as well. The finished molecules are then written to xyz files, containing the elements and the coordinates (corrected for periodicity).
So far, only xyz coordinates of atoms were stored. If one wants to detect which molecules are in the system and how many of them, xyz coordinates alone are not sufficient. Instead, the SMILES (Simplified Molecular Input Line Entry Specification) formate can be used [**?**]. It is essentially an unique specifier for molecules in a single text line (examples are acetic acid: `CC(=O)O` and t-butanol: `CC(C)(C)O`).
After the xyz coordinates of the new molecule are stored, they are converted to the SMILES formate with the `openbabel` program [**?**]. This SMILES string is then compared with a database of already converted molecules. If the string is identical to one of the previous, the number of molecules identified with this string is incremented by one. If no string in the database matches the current (or if the database is still empty), a new entry is generated.
With this method, it is possible to automatically setup a list of individual molecules and (after sorting the final database) give them ordered by abundancy. All SMILES entries in the database are finally reconverted to xyz coordinates for a better visualization of the structures.
The numbers of the different molecular species are added over all frames of the MD, thus giving an indication which species are the most important when averaging over the whole simulation time. Additionally, the numbers of the molecular species in each MD time frame are written to file, ordered with respect to the total abundancies.
In fig. S24 and S19, the 24 most abundant molecules (with seven atoms or less) during the ReaxFF simulation are given for both systems (instead of 12 in the main publication).
Additional information might be gained from the spatial distribution of the molecules. Since the number of molecular species present at one point in time is quite small, plotting a spatially resolved distribution of them for, e.g., the last time frame is of little use. The distributions are shown here for five intervals of the total simulation time.

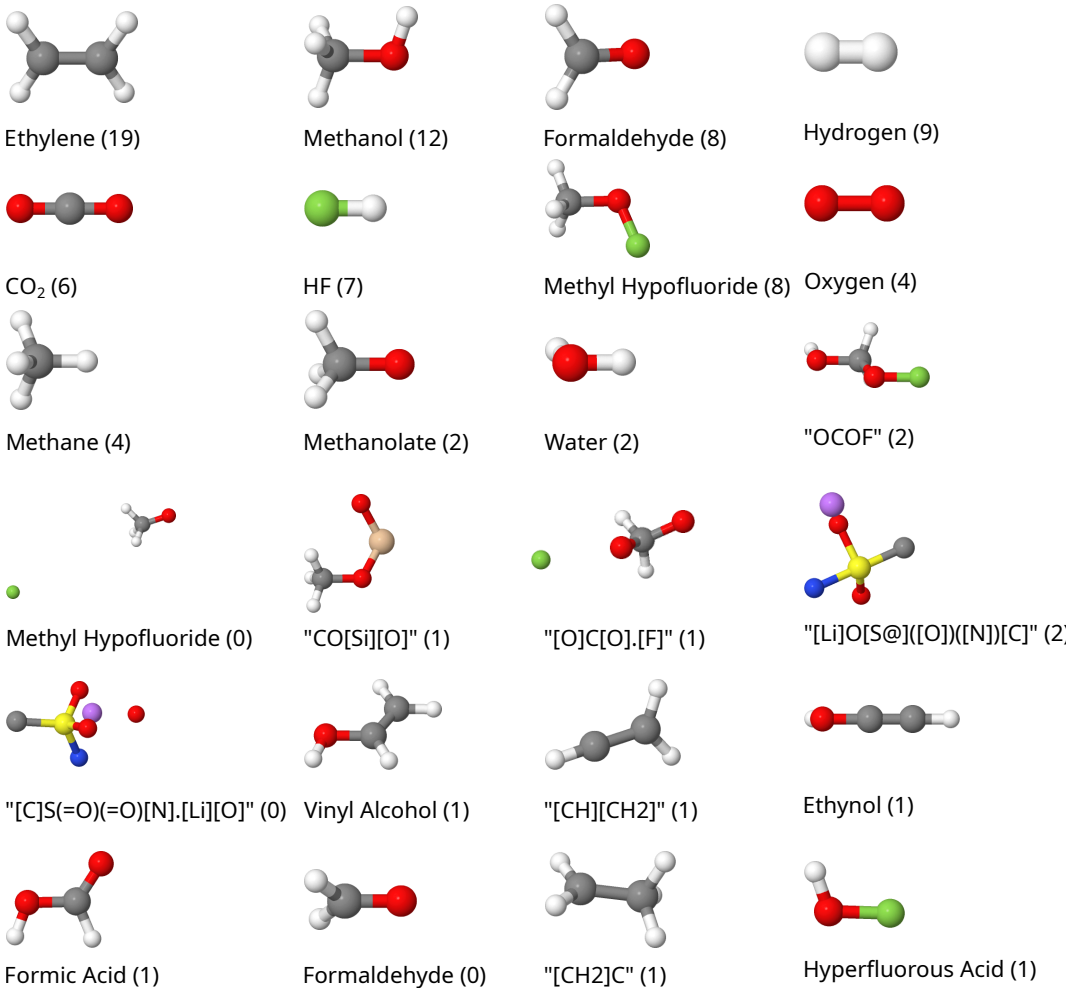

Figure S18: The 24 most abundant molecules or short-lived intermediates during the reactive dynamics with a 0.7 M TFSI concentration at 300 K. Noted in brackets are their numbers in the system at the last trajectory frame. For (probably) short-lived intermediates with unusual bonding patterns, the SMILES strings are given instead of names.

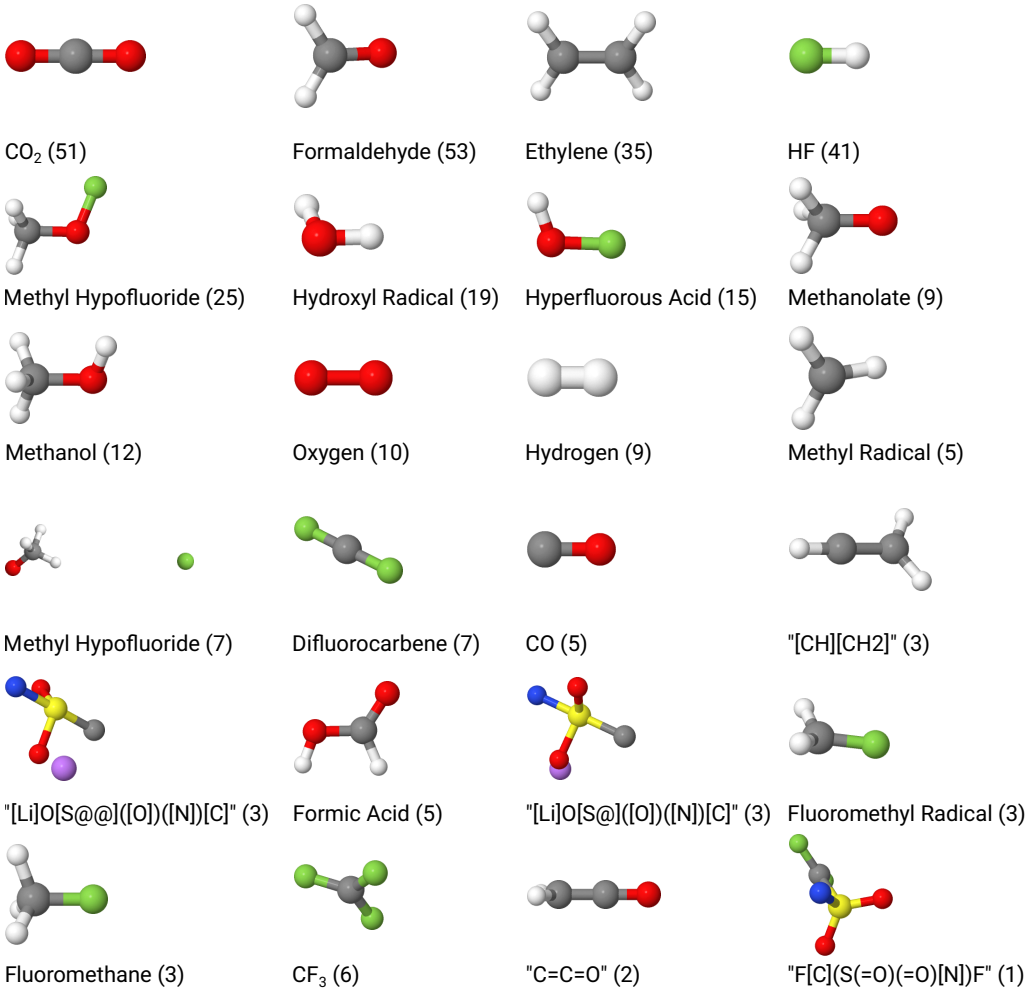

Figure S19: The 24 most abundant molecules or short-lived intermediates during the reactive dynamics with a 4 M TFSI concentration at 300 K. Noted in brackets are their numbers in the system at the last trajectory frame. For (probably) short-lived intermediates with unusual bonding patterns, the SMILES strings are given instead of names.

These distributions are plotted in fig. S20 for the 0.7 M system. As could be expected from the previous findings, there is little variation between (b) and (e), since the SEI formation is essentially finished after ca. 0.4 ns. Between (a) and (b), the number of molecules rises, since the buildup is still in progress. All molecules besides oxygen can only be found in the SEI region, the oxygen originates presumably from local defects in the amorphous SiO_2 structure, where excess oxygen atoms dimerize. The SEI region itself is somewhat shifted towards larger z values when comparing it to, e.g., the bond concentrations shown in the main publication. There we see that the SEI spreads from z=40 to z=60. Small molecules are thus preferentially formed at the electrolyte side of the SEI. The anode side presumably consists mainly of larger networks of molecule parts attached to the dangling SiO_2 chains. Within the SEI region consisting of small molecules, a fine structure can be found, with the methanol molecules nearer to the anode side (z=50 to z=57) and the formaldehyde molecules nearer to the electrolyte side. The most abundant ethylene can be found most probably in the center of the molecular SEI.
If we compare the findings with the time-dependent distributions for the 4 M system in fig. S21, we see as expected a much broader SEI. In the first fifth of the trajectory, the SEI covers essentially the same region as for the 0.7 M system, but it grows further and shortly after small molecules can be found in almost the entire electrolyte region. Concerning the different species, carbon dioxide is preferentially located near the anode, whereas formaldehyde, ethylene and methanolate are spread far into the electrolye region.
We can thus follow that the SEI consists of some kind of layered structure: small molecules are preferentially located at the electrolyte side, with different molecules staying at different layers of the molecular SEI, in contrast to the rather solid state SEI at the anode side.

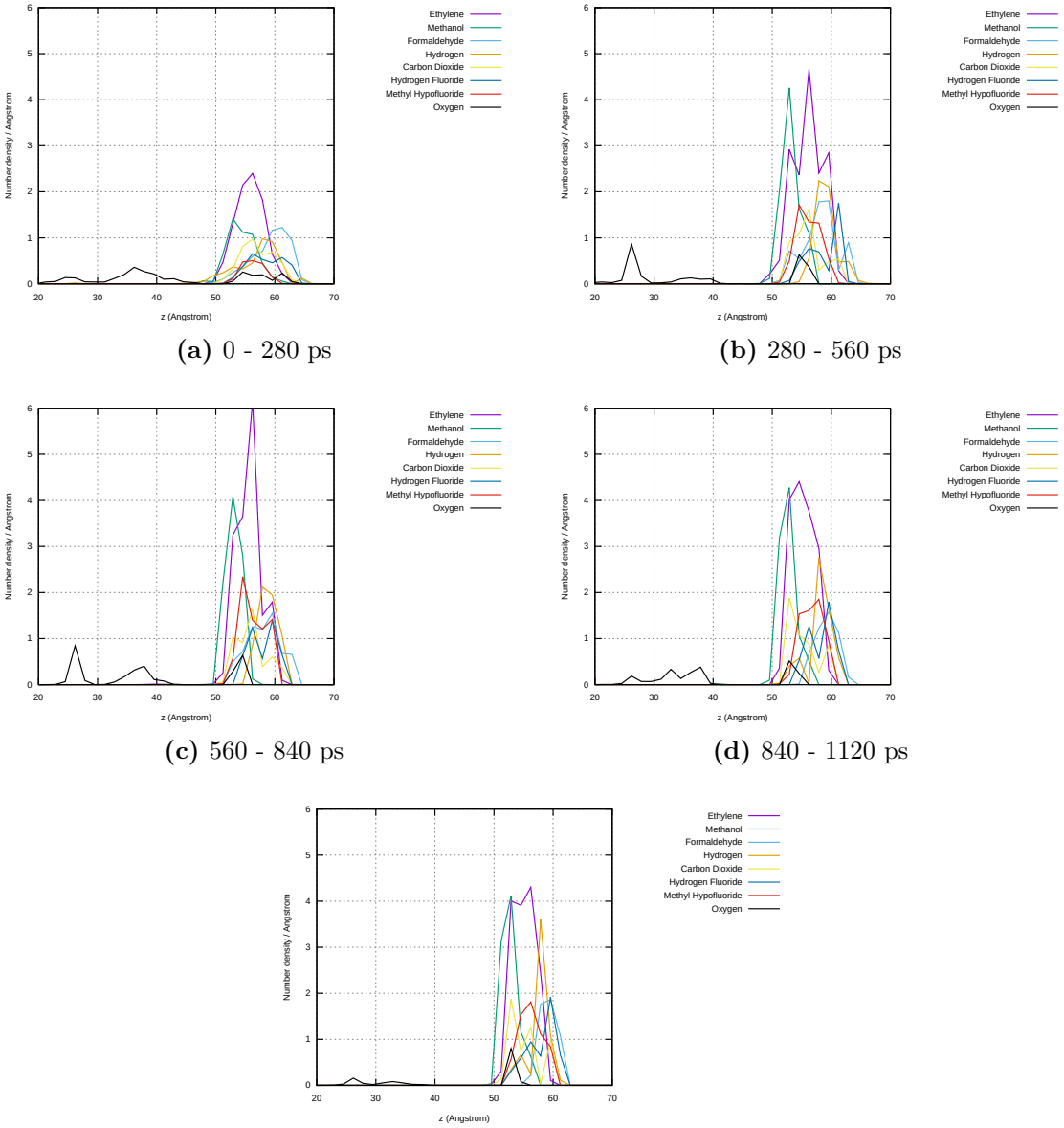

(a) 0 - 280 ps

(b) 280 - 560 ps

(c) 560 - 840 ps

(d) 840 - 1120 ps

(e) 1120 - 1400 ps

Figure S20: Space-resolved concentrations of the most abundant 8 molecule species, averaged over five phases of the overall dynamics (0.7 M TFSI).

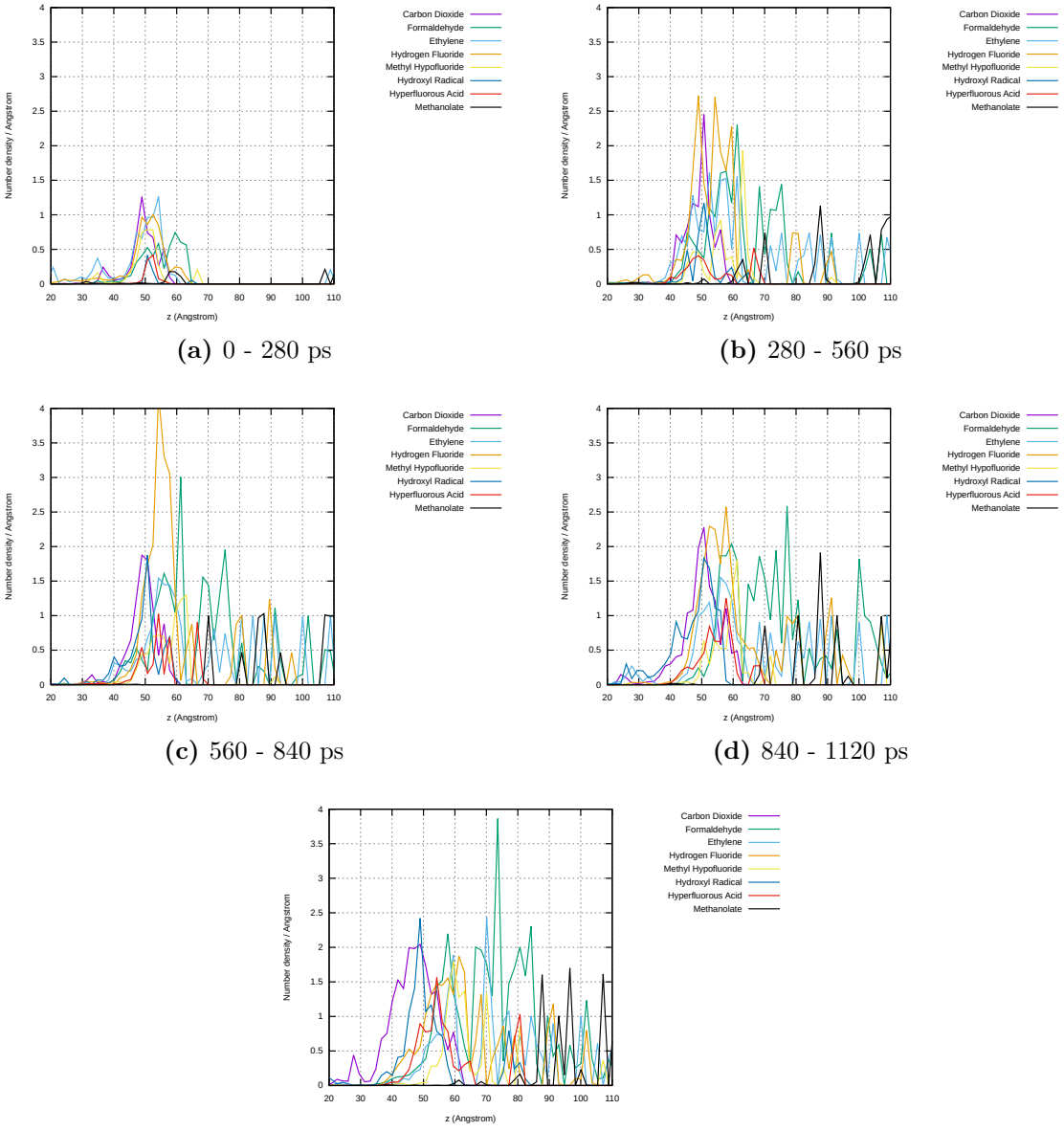

(a) 0 - 280 ps

(b) 280 - 560 ps

(c) 560 - 840 ps

(d) 840 - 1120 ps

(e) 1120 - 1400 ps

Figure S21: Space-resolved concentrations of the most abundant 8 molecule species, averaged over five phases of the overall dynamics (4 M TFSI).

4 Experimental Results

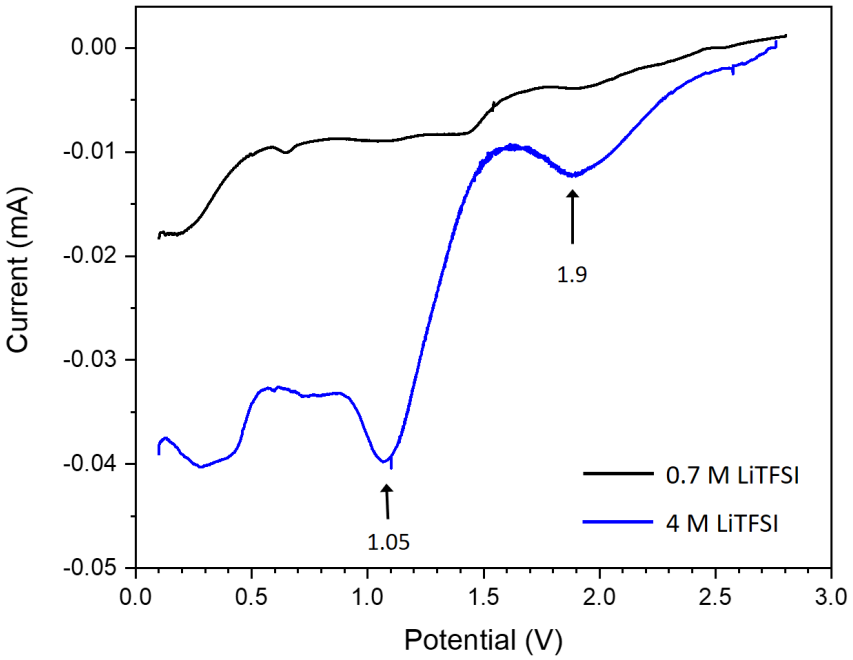

Figure S22: Displays cyclic voltammetry measurements obtained by a decrease in the voltage the open circuit potential to 0.1 V for 0.7 M (black) and 4 M LiTFSI (blue). Significant peaks are marked on the figure.

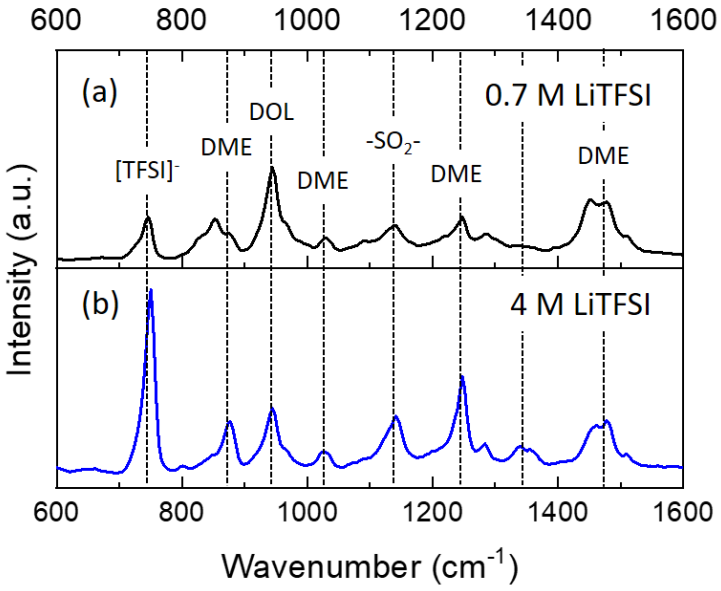

Figure S23: Displays the Raman spectra obtained for the electrolyte series with increasing LiTFSI concentration: (a) 0.7 M LiTFSI and (b) 4 M LiTFSI in 2:1 DME:DOL (v/v). The significant peaks are noted on the figure.

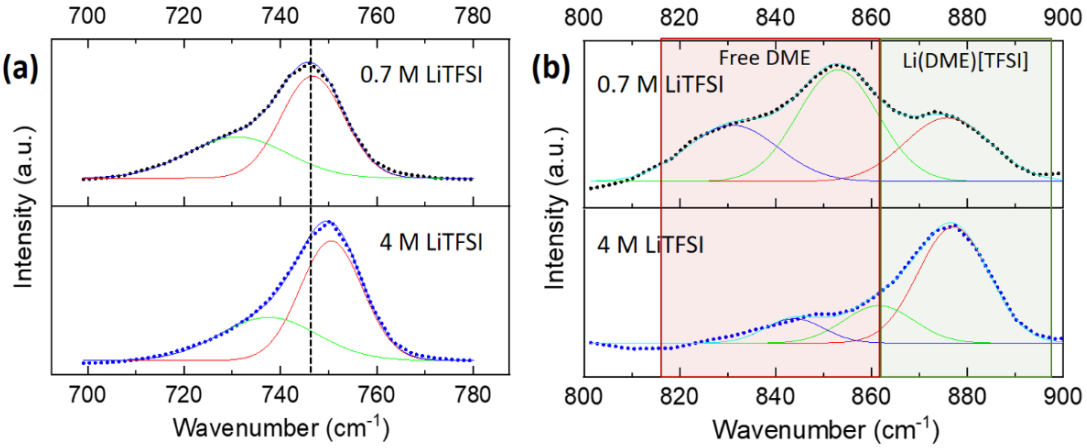

Figure S24: Displays the bands between 700-780 cm-1, characteristic of the vibrations of [TFSI]- (a) and the bands between 800-900 cm-1, characteristic of the CH2 vibrations of monoglyme or dimethoxyethane (DME) (b).

Table S2: Displays peak assignments from resolved XPS spectra and their respective binding energies (eV) and percentage (%).

		Pristine PorSi		**PorSi in 0.7 M**		**PorSi in 4 M**	
Element	**Assignment**	**BE (eV)**	**%**	**BE (eV)**	**%**	**BE (eV)**	**%**
C 1s	Lithiated C	-	-	-	-	283.2	0.8
	C-H / C-C	284.2	11.3	284.8	59.3	285	43.0
	CH_2-$CH_2OR)$-$_n$ / $(CH_2$-CH_2-$OCH_2O)$-$_n$	285.6/ 287.2	49.3/ 36.9	286.4	20.2	286.8	24.5
	$CH_2CH_2OCH_2O$	288.6	2.5	288.8	18.9	-	-
	HCO_3Li	-	-	-	-	289.4	15.8
	CF_2	-	-	292.5	1.6	292.9	15.9
O 1s	Lithiated O	-	-	529.9	16.0	530.7	20.8
	Organic C-O	-	-	531.7	76.4	532.5	68.8
	Organic C=O / Si-O	533.5	100.0	533.7	7.6	534.1	10.4
N 1s	Unsure	-	-	398.9	100.0	399.1	79.8
	Unsure	-	-	-	-	401.6	20.2
F 1s	LiF	-	-	685.1	40.0	685.6	32.1
	SO_2CF_3 / $Li_xS_2F_y$	-	-	688.9	60.0	689.2	67.9
S 2p	N-SO_2CF_3 / $LI_2S_2O_4$	-	-	166.5	20.5	166.8	20.7
	$SO_3^{(2-)}$	-	-	168.4	79.5	168.7	79.3
Si 2p	c-Si	99.4	47.7	-	-	-	-
	Org. Si / a-Si	100.7	8.9	100.6	100.0	101.8	100.0
	SiO_x	103.5	43.4	-	-	-	-
Li 1s	Org. Li / LiTFSI	-	-	54.6	90.9	55.4	100.0
	LiF	-	-	56.2	9.1	-	-

Table S3: Displays elemental percentages determined from resolved XPS spectra. Note that Li 1s percentages were not included.

Element	**Pristine PorSi (%)**	PorSi in 0.7 M (%)	PorSi in 4 M (%)
C 1s	28.4	36.6	16.8
O 1s	37.5	47.0	32.1
N 1s	-	1.5	10.1
F 1s	-	5.8	15.4
S 2p	-	2.1	7.1
Si 2p	34.2	11.4	14.4